Free dendrite growth in undercooled melts: experiments and modeling *Edited by*
TMS (The Minerals, Metals & Materials Society), 2004

FREE DENDRITE GROWTH IN UNDERCOOLED MELTS: EXPERIMENTS AND MODELING

Dieter M. Herlach, Oliver Funke, Phanikumar Gandham, Peter Galenko

Institut für Raumsimulation, DLR, D-51170 Köln, Germany

Keywords: Containerless processing, undercooling of materials, dendritic growth, non-equilibrium solidification

Abstract

Essential progress of modeling of free dendrite growth in undercooled melts was achieved by the ”classic” work of Wilfried Kurz et al. In the present paper, recent developments in experimental methods are described to measure the dendrite growth dynamics in undercooled metallic melts, which are containerlessly processed by electromagnetic levitation technique. Results of essentially improved accuracy in measuring the dendrite growth velocity as a function of undercooling are presented for “nominally” pure nickel. In parallel, the sharp interface dendrite growth theory is extended to include effects both of melt convection and electromagnetically induced stirring of the levitation processed liquid. The analysis of the results indicate that fluid flow causes an enhancement of the dendrite velocity in the small undercooling range. Also, small amounts of impurities in nickel can lead to an increase of the growth velocity but with a temperature characteristics being different from that of the effect by fluid flow. This allows to discriminate between both contributions as it is shown by experimental investigations and modeling within the extended sharp interface model and phase field modeling as well.

Introduction

The mode of dendritic growth is of essential interest in manifold dynamic processes in inorganic as well as in organic materials. In particular, it is of great practical importance in solidification processes of metallic materials as casting, welding, surface re-solidification, melt spinning and others. The formation of dendrites in melts is an example of self-organized formation of structures. Worldwide 10^{13} dendrites per second are formed during casting of metals. Since the dendritic morphology controls the microstructure evolution of a material it is of great importance in designing metallic materials with respect to their physical and chemical properties and quality for users. Concerning solidification one distinguishes between near-equilibrium and non-equilibrium conditions. In the former case as present in directional solidification cooperative dendritic growth occurs due to constitutional undercooling effects while in the latter case one deals with equiaxed free growth of dendrites in undercooled melts. Here, the undercooled melt acts as a heat sink for the released heat of crystallization of a growing solid dendrite.

The efforts to date are directed towards a quantitative description of dendrite growth dynamics in metallic melts in order to develop a predictive capability for the design of materials from the liquid state. Such quantitative modeling requires both reliable physical models for dendrite growth dynamics and accurate experimental investigations of the growth dynamics as well. Concerning the theoretical description of equiaxed dendrite growth also under the con-

ditions far away from equilibrium, the pioneering work of Wilfried Kurz et al. gave access to analytical treatment of dendritic growth in undercooled melts [1]. The sharp interface model describes dendritic growth in terms of thermal and chemical Peclét numbers, P_t and P_c, respectively. This means, the product of dendrite growth velocity V and dendrite tip radius R is correlated to the undercooling ΔT. In order to achieve a unique relation of all three variables the result of the marginal stability analysis was utilized for a long time, which delivers an independent equation for the tip radius R [2]. Originally, the dendrite growth theory was developed for conditions of local equilibrium at the solid-liquid interface. By an extension, these conditions were relaxed by taking into account a kinetic interface undercooling and deviations from chemical equilibrium at the solidification front of alloys [3]. The latter one is described by a velocity dependent partition coefficient k(V) according to the solute trapping model by Aziz [4]. As a further extension, not only deviations from local equilibrium at the interface but also in the bulk melt near by the interface are taken into account [5].

At the same time experimental techniques were developed to measure quantitatively the dendrite growth velocity as a function of undercooling on levitation processed drops [6, 7]. In these experiments metallic drops were melted and containerlessly undercooled and solidified. The growth velocity was determined by measuring the time needed by the solidification front to propagate through the entire sample through a well-defined observation window [**7**]. In the present work measurements of the dendrite growth velocity on nominally pure nickel are presented. Experimental results are obtained by employing three different experimental techniques, which deliver data of high accuracy and good reproducibility at small, medium and high undercoolings. The experimental results are analyzed within the sharp interface model based upon the work of Wilfried Kurz et al. This model was extended by including effects of mass and heat transport due to fluid flow motion caused by convection and electromagnetic stirring of levitated melts and applying solvability theory for the independent determination of the dendrite tip radius. These results are compared with experimental data and predictions of phase field modeling.

Experiments

Undercoolings of pure transition metals up to several hundred degree centigrade are achieved by the application of electro-magnetic levitation techniques the details of which are described in detail elsewhere [8]. Photo sensors (PS) are used to measure the dendrite growth velocity of levitation undercooled melts. Figure 1 shows the experimental set up. The photo-sensors are arranged perpendicular to the symmetry axis of the coil. The solidification of the sample is externally nucleated by a trigger needle, which is touching the surface of the sample at its bottom. Solidification starts at this point and the dendrites propagate isotropically through the volume of the sample. A small part of the equatorial sample surface is imaged by an optical system on the sensitive area of the photodiodes. The growth velocity, V, is obtained by dividing the solidification pathway, Δs, by the measured time, Δt, needed by the solidification front to propagate through the observation window, $V = \Delta s/\Delta t$. Thereby, it is assumed that the solidification front can be approximated by the envelope of the dendrite tips. This assumption is justified at medium and particularly at high undercoolings, where many small dendrites are formed, but it is violated at small undercoolings where only a few thick dendrites are propagating through the melt. Accordingly, the scatter and uncertainty of the measurements by using the PS are increasing with decreasing undercooling.

To measure the dendrite growth velocity at small and medium undercoolings also with high reliability and reproducibility, we developed a capacity proximity sensor (CPS) [9]. The set up is schematically illustrated in Figure 1. It consists of a nucleation trigger needle made of the same material as the sample. The needle is part of a resistance - capacitance (RC) electrical circuit whose resonance frequency is measured. If the needle is touching the sample and

initiates solidification, the capacitance of the RC – circuit changes abruptly. The time, t_1, of initiating crystallization is measured by a sudden change of the output signal of the RC circuit with a time resolution of 1 μs. The counterpart of the triggering point at the opposite side of the sample is focused by an optical system on the sensitive area of a photodiode. As soon as the central dendrite is arriving at the top of the sample at time, t_2, the signal of the photodiode rapidly increases. The growth velocity, V, is then obtained by dividing the height of the as-solidified sample, D_o, by the time difference $\Delta t = t_2 - t_1$: $V = D_o/\Delta t$.

In addition to PS and CPS, we also apply a high-speed digital camera to observe the propagation of the solidification front. The camera enables observations of the solidification process at frame rates of up to 120,000 frames per second (fps) at a resolution of 128×16 pixel. For the dendrite growth velocities during solidification of an undercooled Ni melt frame rates of 30,000 fps have proven in a first test to be a good choice for low and medium undercoolings. This frame rate offers a higher resolution of 256×128 pixel. Figure 2 gives a sequence of pictures taken during solidification of a Ni sample undercooled by ΔT = 90 K (upper part) and undercooled by ΔT = 140 K (lower part), respectively [10]. It can be seen that the solidification front at the sample surface is of an irregular shape for ΔT = 90 K, while at ΔT = 140 K the front appears very smooth.

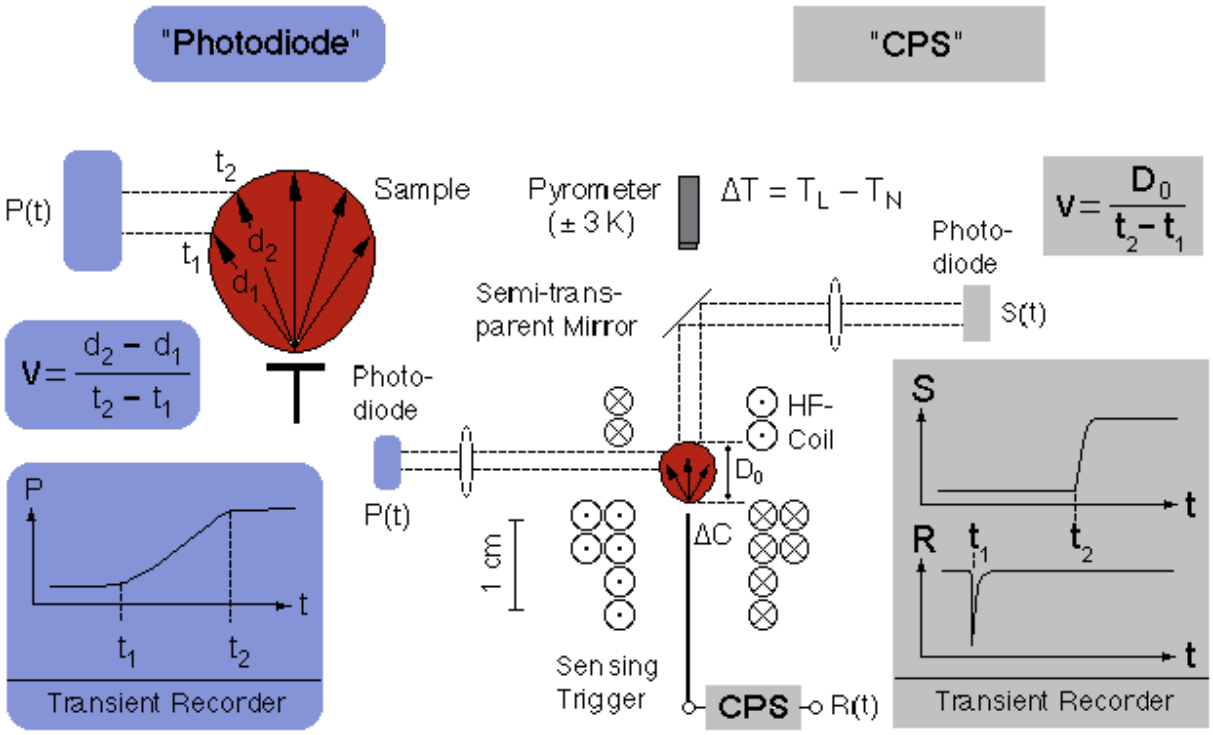

Figure 1: Experimental techniques to measure the growth dynamics of the solidification front in levitation undercooled samples: the photodiode method (left hand side) and the capacity sensor technique, CPS (right hand side).

Present measurements of dendrite growth velocities in undercooled levitated nickel melts were performed for six individual samples of different masses (1.0 g < m < 1.5 g) by using an improved CPS technique [10]. The experiments provide a data set of dendrite growth velocities covering the range of undercoolings from 30 K < ΔT < 260 K. In Figure 3 the present CPS data is shown together with two other data sets: as obtained with a similar CPS technique by Eckler and Herlach previously [11] and with a high-speed camera by Matson [12], respectively. All three data sets are differing from each other. Beginning at ΔT ≈ 65 K the growth velocity values in the present CPS data are deviating from the previous CPS data to *higher values* for 65 K < ΔT < 180 K. The region of maximum discrepancy between both data sets is found in the interval 105 K < ΔT < 132 K. In the previous CPS data set this region is followed

by a steep increase in the velocity accretion with increasing undercooling, resulting in a merge of both CPS data sets at approximately $\Delta T \approx 180$ K. At $\Delta T < 65$ K as well as at $\Delta T > 180$ K both CPS data sets are in good agreement. In comparison with the camera data of Matson et al. [12] the present CPS data shows a deviation to *lower growth velocities*, starting already at $\Delta T \approx 55$ K, and both data sets are in agreement at $\Delta T \geq 165$ K.

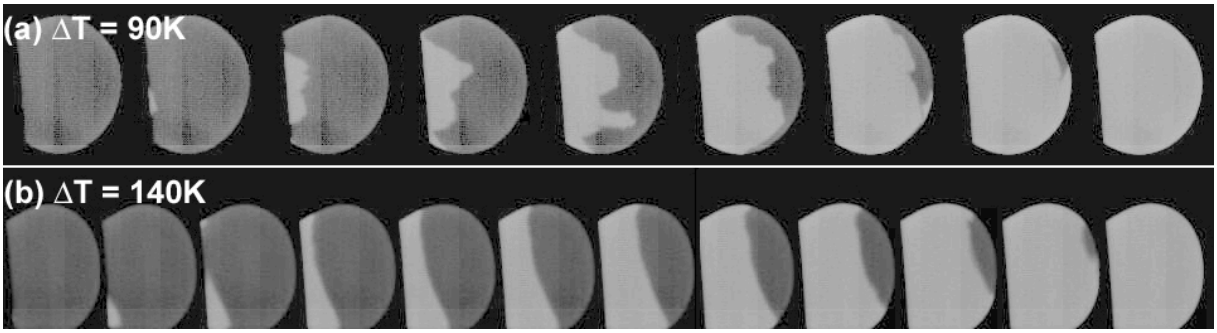

Figure 2: Propagation of the solidification front (light gray) through an undercooled Ni melt (dark gray) for $\Delta T \approx 90$ K *(a)* and $\Delta T \approx 140$ K (b). Both sequences were recorded at a frame rate of 30,000 fps, for 90 K only each fifth image is shown. Triggering occurred at the bottom of the sample, which is to the left in this display. A small part (≈ 15%) of the sample's bottom part is hidden by the coil. A clear difference in the appearance of the solidification front in both image sequences can be seen.

There is a clear discrepancy in both CPS data sets, intimating that an effect might be responsible for the discrepancy that is independent from the experimental technique/hardware. In order to demonstrate more clearly the different growth velocity versus undercooling dependence, all three data sets are plotted in a double logarithmic diagram, and a third order polynomial was fitted to each of the data sets. As can be seen from Figure 3, both the present CPS data and the camera data by Matson et al. [12] show a rather monotonous increase (following a power law) until the breakpoint at $\Delta T^* \approx 180$ K is reached, at which the temperature dependence of $V(\Delta T)$ changes. On the contrary, the previous CPS data reveals a distinct change in the velocity/undercooling relationship at $\Delta T < \Delta T^*$.

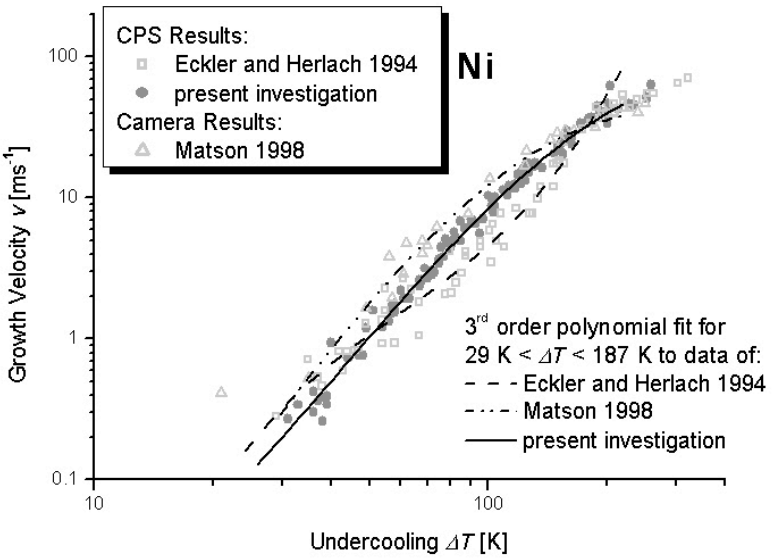

Figure 3: All three data sets under consideration in double logarithmic diagram [10]. Also shown are the results of a third order polynomial fit to each of the three independent data sets. It can be seen that the velocity accretion with increasing undercooling is rather monotonous for Matson's data [12] as well as for the present CPS data, while a clear change of the velocity – under-cooling characteristics can be seen in the previous CPS data by Eckler and Herlach [11].

In order to find an explanation for the observed discrepancies in the data sets we analyzed the Ni samples that were used in our investigation for their purity by chemical spectroscopy. The outcome of this analysis as an average of investigations of four different samples is given in Table 1. The overall amount of impurities is in the order of 0.01at%, with carbon as the main

constituent of the impurities. Carbon, if not being present in the sample at time of distribution of the Ni rod, might be introduced to the sample during the process of sample cutting – before and after levitation – although each sample was cleaned with Propanol before each experiment. The results of the chemical purity analysis may suggest that the samples even though prepared from Ni of nominal purity of 99.99 may contain a slightly higher amount of impurities than 99.99 in particular if also non-metallic elements are taken into account. When impurities show a very small partition coefficient when alloying to nickel they may influence the dendrite growth dynamics seriously even at very small concentration. The essential influence of strongly partitioning elements on the dendrite growth dynamics when adding to pure Ni has been shown by measurements on dilute Ni-B [13] and Ni-Zr [14] alloys. The degree of impurities might vary between individual samples. This could explain the higher degree of scattering present in the previous CPS data.

Table 1: Results of chemical analysis of sample purity. Due to the use of a HeH_2 -gas as protection atmosphere and for the sample cooling, the amount of O_2 has decreased during experiment by a factor of two while the content of H_2 has increased by a factor of five. It can be seen that the overall purity of the sample has been improved during the course of the experiment.

Ni	**O_2 ppm**	**H_2 ppm**	**C ppm**	**Si ppm**	**Fe ppm**	**Co ppm**	**Total ppm (at%)**
unprocessed	19.2	0.75	56	18	4	2	99.95 (0.009995)
processed	10.4	3.86	49	10	3	3	79.26 (0.007926)
average	14.8	2.305	52.5	14	3.5	2.5	89.61 (0.0089.61)

Sharp interface model for dendrite growth in levitation processed drops

Electromagnetic levitation exhibits complicated phenomena of interaction of heat transport and electromagnetic fields with the existing moving solid-liquid interface. For instance, heating and cooling of a droplet, the flow of the induced current, the inclusion of the liquid phase of the droplet into the forced flow due to the Lorentz force caused by the alternating electromagnetic field, and the solidification process itself lead to these complicated phenomena [15]. The situation of forces acting on levitated drops is sketched in Figure 4.

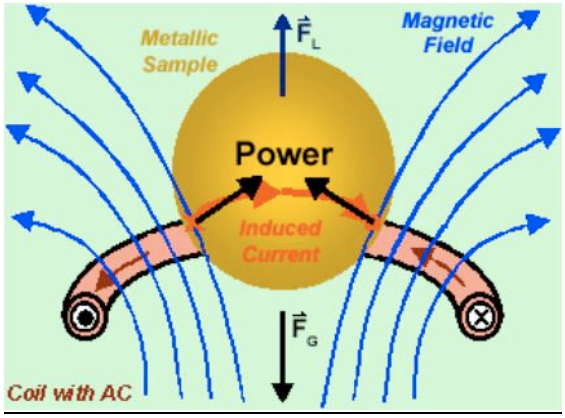

Figure 4: A metallic sample, which is placed into an alternating electromagnetic field as present in a levitation coil, which is represented by one copper winding. The alternating electromagnetic field causes a levitation force F_L that counteracts the gravitational force F_G and leads to levitation if $F_L = F_G$. Simultaneously, the alternating magnetic field induces eddy currents, which heat up the sample but also produce strong electromagnetically induced stirring, which changes the conditions of heat and mass transport in the liquid sample in addition to natural convection.

The influence of an external forced flow imposed on the growing dendrite in undercooled pure melt has been treated theoretically during the past two decades [16, 17, 18, 19, 20, 21]. Taking into account the effect of forced convective flow on dendritic growth in a levitated

droplet the LGK/LKT model [22, 23, 3] has been modified and extended [15]. Following the extended model, the final system of equations can be presented as follows.

We consider an axi-symmetric parabolic shape of the dendrite tip, which has the interface temperature T_i and propagates into the undercooled melt with the constant velocity V. The total undercooling $\Delta T = T_L - T_\infty$ at the dendrite tip of a pure metal consists of the following contributions:

$$\Delta T = \Delta T_T + \Delta T_R + \Delta T_K \tag{1}$$

Here: $\Delta T_T = T_i - T$ is the thermal undercooling for removal of the latent heat released at the dendrite tip and it is described by

$$\Delta T_T = T_Q Pe_g \cdot \exp(Pe_g + Pe_f) \cdot \int_1^\infty \xi^{-1} \cdot \exp\left[-\xi Pe_g + (\ln \xi - \xi) Pe_f\right] d\xi \tag{2}$$

where R is the tip radius of the parabolic dendrite, T_Q is the adiabatic temperature of solidification, $Pe_g = V R/(2a)$ is the thermal Péclet number, $Pe_f = U_o R/(2a)$ is the flow Péclet number; U_o is the velocity of the uniformly forced flow far from the dendrite tip, and a is the thermal diffusivity. The flow velocity U_o can be defined from a special consideration of the energy balance for the energies of the electromagnetic field, the gravitational field, and the viscous dissipation [15]. This yields

$$U_o = \left[\frac{2}{\rho}\left(\frac{\mu}{\rho} g R_o + \frac{B_o^2 (1 - \exp(-2R_o/\delta))}{8\pi}\right) + \frac{\omega^2 \delta^2}{2}\right]^{1/2} \tag{3}$$

where g is the modulus of vector of the gravity acceleration, ρ is the mass density and μ is the dynamic viscosity of the liquid phase. In this case, the velocity U_o included in the thermal undercooling (2) as a free parameter becomes now independently defined from Eq. (3) for the *EML* process.

The penetration depth δ of the electromagnetic field in Eq. (3) is considered as a skin depth of the surrounding high frequency magnetic field into the sample and hence the region where the induced eddy current provides for the heating. The skin depth δ is defined by the electric and magnetic parameters as follows:

$$\delta = \left[\frac{2}{\omega \sigma_g \mu_o}\right]^{1/2} \tag{4}$$

where σ_g is the electric conductivity (measured under isothermal conditions), μ_o is the magnetic permeability, and ω is the frequency of the applied current. δ is considered as a skin depth for the alternating magnetic field in the liquid droplet, which decreases for a short distance at which the magnetic field decays exponentially

$$|B| = B_o \cdot \exp\left[(r - R_o)/\delta\right]$$

where $|B|$ is the modulus of the magnetic induction vector, B_o is the time averaged value of the magnetic induction, and r is the radial distance of a droplet of the radius R_o.

In Eq. (1), the curvature undercooling ΔT_R due to the Gibbs-Thomson effect is described by

$$\Delta T_R = 2\Gamma(1 - \varepsilon_4 \cos 4\varphi)/R \tag{5}$$

where Γ is the capillary constant (Gibbs-Thomson parameter), ε_4 is the parameter of anisotropy of the surface energy, and φ is the angle between the normal to the interface and the direction of growth along the z-axis. The kinetic undercooling ΔT_K which is necessary for the attachment of atoms to the interface is described by

$$\Delta T_K = V/\mu_K, \quad \mu_K = \mu_{K0}(1 - \varepsilon_K \cos 4\varphi) \tag{6}$$

where μ_K is the kinetic coefficient for growth of the dendrite tip, ε_K is the parameter of anisotropy for the growth kinetics.

Taking into account Eqs.(1) - (6), it results a single equation for the dendrite tip velocity V and dendrite tip radius R. From solvability theory, an independent expression for the dendrite tip radius R is obtained [18]

$$R = \frac{\Gamma}{\sigma^* T_Q Pe_g} \tag{7}$$

with the stability parameter σ^* given by

$$\sigma^* = \sigma_o \cdot \delta_c^{7/4} \left[1 + \beta(\mathrm{Re}) \frac{U_o \Gamma}{a T_Q}\right]^{-1} \tag{8}$$

where σ_o is a constant; $Re = U_o R/\nu$ is the Reynolds number. The function β(Re) can be found from Ref. [18] (with adaptation of the analytical results to the 3D solution). For computation of the stability parameter σ^* we choose the results of phase-field modeling [20] accordingly with

$$\sigma_o \delta_c^{7/4} / \sigma^* = 1.675$$

for the 3D upstream fluid flow imposed on the scale of a freely growing dendrite.

Note that the selection criterion for the growth mode given by Eqs.(7) - (8) is only true for the relatively small undercoolings, i.e. when the direction of growth of the dendrite is dictated by the anisotropy of surface energy and the imposed direction of the liquid flow. Obviously, when the solidification of a stagnant undercooled melt occurs, i.e. with $U_o = 0$, and for the isotropic surface energy and growth kinetics, i.e. with $\varepsilon_\gamma = 0$ and $\varepsilon_K = 0$, one gets the LKT model [3] as a partial limit for Eqs. (1)-(8). Thus, from the system of two main equations (1) and (7) the velocity V and tip radius R of the dendrite can be calculated as a function of the initial undercooling ΔT.

Results on "nominally" pure Ni

We have shown [15] that the inclusion of a forced convective flow into the model of dendritic growth gives partially satisfactory description of experimental data at small undercoolings previously obtained by Eckler and Herlach utilizing the CPS technique [11]. Now we compare the predictions of the present model Eqs. (1)-(8) with the new results (cf. Figure 5) on dendritic growth velocity on nominally pure Ni as measured by an improved CPS technique of the present work.

The analysis of Brener [24, 25] and Brener and Melinikov [26] shows that, for a pure system solidifying at higher undercooling, the anisotropy of kinetics plays a crucial role in selection of the dendritic growth mode. This model can be taken from Eqs. (1)-(6) as the limiting case of $U_o = 0$ and with the selection criterion for the growth mode consistent with both the anisotropies of surface energy and growth kinetics. The parameters of anisotropy ε_γ and ε_K are taken from data of atomistic simulations of Hoyt et al. [27, 28], which have been linked recently with the phase-field simulations of Bragard et al. [29] for analysis of dendritic growth in a wide range of undercoolings. The values for the atomic kinetic growth coefficient as resulting from atomistic simulations are lower for approximately 4-5 times than predicted by the collision-limited theory of Coriell and Turnbull [30]. The former values are rather well compared with the values found from previous molecular-dynamic simulation data of Broughton et al. [31]. Also, to adjust the kinetics of rapid dendritic growth of nickel based alloys, Galenko and Danilov [5, 32] found agreement between experiment and theory only if the kinetic under-

cooling ΔT_k is assumed to be by a factor of 5 larger than predicted by the theory of collision-limited growth. These findings might be explained due to more complicated behavior of the atomic attachment kinetics at the solid-liquid interface. To model dendrite growth kinetics of nickel, material parameters are used as given in Table 2.

As Figure 5 illustrates, Brener's theory without convection [24, 25] leads to deviations from the experimental data at small undercoolings $\Delta T < 100$ K whereas it predicts the experimental data quite well at higher undercoolings $\Delta T > 150$ K. This finding confirms the assumption that the convection enhances the dendrite growth velocity at small undercoolings and shows the essential role of anisotropy of the growth kinetics at higher undercoolings.

Table 2: Material's parameters of nickel and characteristics of the electromagnetic facility used in calculations.

Parameter	Symbol	Numerical value
Adiabatic temperature	T_Q	418 [K]
Density	ρ	$8.1 \cdot 10^3$ [kg/m^3]
Dynamic viscosity	μ	$4.3 \cdot 10^{-3}$ [Pa•s]
Thermal diffusivity	a	$1.2 \cdot 10^{-5}$ [m^2/s]
Gibbs-Thomson parameter	Γ_o	$3.4 \cdot 10^{-7}$ [K•m]
Angle between the normal to the interface and the dendrite growth direction	φ	0 [deg]
Parameter of anisotropy of surface energy	δ_ε	$1.8 \cdot 10^{-2}$ [-]
Parameter of kinetic anisotropy (taken for the theory [27])	δ_k	$1.3 \cdot 10^{-1}$ [-]
Electric conductivity	σ_R	$4.1 \cdot 10^6$ [Ω•m]
Magnetic permeability	μ_o	$4\pi \cdot 10^{-7}$ [H/m]
Frequency of the applied current	ω	$3.0 \cdot 10^5$ [Hz]

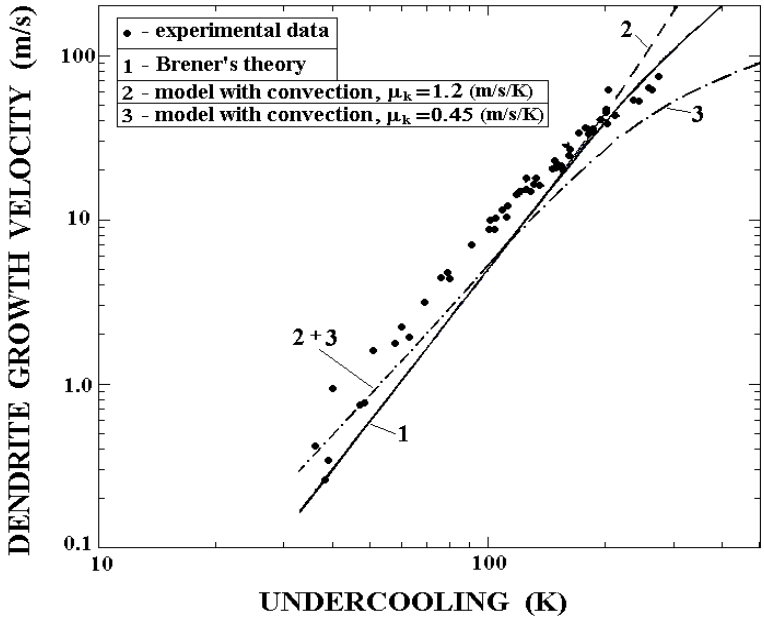

Figure 5. Comparison of model predictions with the experimental data on dendrite tip growth for pure Ni. The solid line 1 shows the effect of anisotropy of kinetics predicted by the analytical theory of Brener [24, 25]. Predictions of the present model are given by the dashed line and dashed-dotted line which represent the effect of convective flow with different isotropic kinetic coefficients. The velocity of upstream flow imposed on dendrite has been calculated from Eqs. (3) and (4) as the value of U_0 = 1.4 m/s.

An inclusion of convection by Eqs.(1)-(8) enhances the dendrite velocity and leads to a partial agreement with experimental data at small undercoolings $\Delta T < 100$ K when the flow has the velocity $U_0 = 1.4$ m/s as one of the limiting speeds for the established assumptions of the present model for the forced flow in laminar regime. This effect of the forced flow on dendritic growth is shown by the curves 2 and 3 in Figure 5. Note that without anisotropy of kinetics

and with the averaged kinetic coefficient μ_k =0.45 (m/s/K) [27, 29] the velocity-undercooling curve 3 deviates significantly from the experimental data at medium and high undercoolings ΔT > 100 K. For the case of ideal collision-limited growth [30] with the averaged kinetic coefficient μ_k =1.2 (m/s/K) the experiment might be described satisfactorily within the medium undercooling range 100 K < ΔT < 180 K. However, as it is known from theory [26, 29], dendrite growth does not occur without crystalline anisotropy, especially, at high undercoolings when the role of the anisotropy of the surface energy vanishes. Therefore as it is shown by the application of the model [26] (see curve 1 in Figure 5), when the effect of the forced flow on the dendritic growth is negligible at medium and high undercoolings, the dendrite velocity is enhancing due to the presence of kinetic anisotropy. The details of modeling results with taking into account effects of convection and both anisotropies of surface energy and kinetics are summarized in the following section.

The phase-field modeling

The phase-field model was suggested and developed for the description of phase transitions in condensed matter with diffuse phase interfaces [33, 34, 35, 36]. In the present investigation, we have used the "thin-interface" analysis of the phase-field model [37, 38] where the interface thickness is assumed to be small compared to the scale of the crystal but not smaller than the microscopic capillary length. The thin-interface limit is ideally suited to model dendritic growth in pure materials quantitatively at low undercooling when used in conjunction with efficient numerical algorithms [38, 39].

The phase-field and energy equations were taken from the model of Karma and Rappel [37, 38] with the momentum and continuity equations of motion of the liquid phase taken from Beckermann et al. [39]. Furthermore, in the momentum equation, the additional force for the motion of the liquid phase in undercooled droplet, i.e. averaged in time Lorentz force, has been introduced. These governing equations have been solved numerically on the uniformed numerical grid with application of the special numerical algorithms. Constants of modeling applicable to the pure nickel and analysis of the results will be presented elsewhere [40].

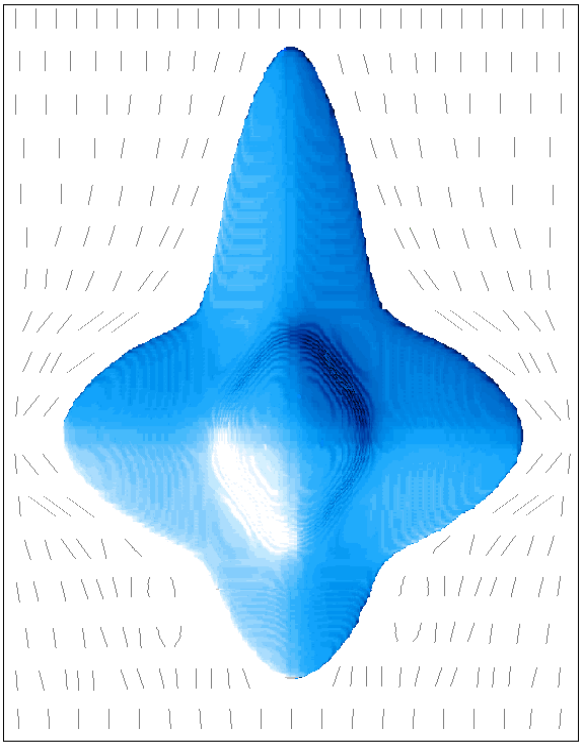

Figure 6. Dendrite growth with convective flow at ΔT = 0.30 and U_0 = 0.7 m/s. Growth velocity V of the up-stream branch is most pronounced in comparison with the down-stream branch due to forced convection with the far field flow speed U_0. The dashed lines around the dendrite indicate the flow velocity vectors in the vertical cross-section.

The phase-field modeling exhibits an increase of the velocity of the up-stream dendrite branch in comparison with the dendrite tip velocity in a stagnant melt (cf. Figure 6). Therefore, for the flow in a levitated droplet, we are expecting an enhanced dendrite velocity, which might decrease the disagreement between experimental data and predictions of theory without convection. Figure 7 shows the quantitative comparison of the predictions of the results of present phase-field modeling with the previous [11] and present (see experimental section of this work) experimental data for growth kinetics of nickel dendrites.

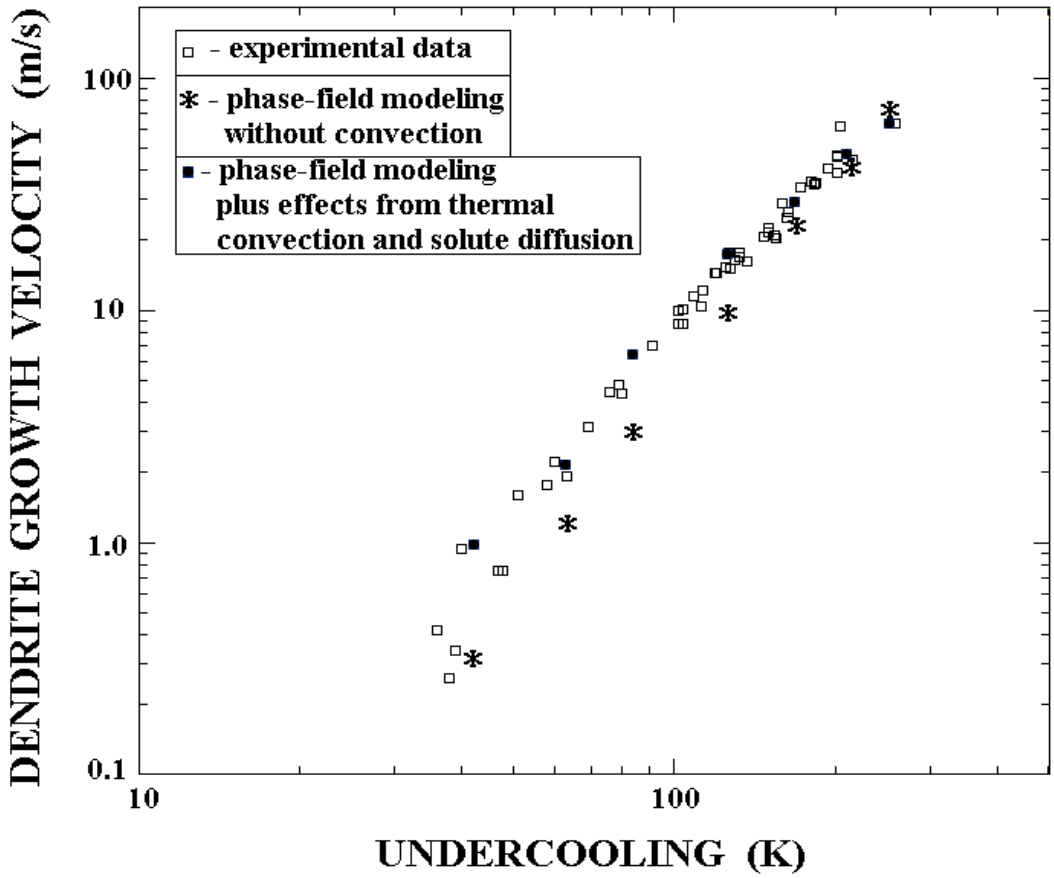

Figure 7. Comparison of the results of the phase-field modeling for pure system in stagnant melt (stars) and the same phase-field modeling with taking inro account the thermal convection and calculated effects from the solute diffusion (filled squares) with the present experimental data on solidification kinetics of Nickel dendrites (open squares).

Our analysis [40] reveals that

(*i*) the dendrite velocity is greater in the direction opposite to the flow (Figure 6), the dendrite growth velocities extracted from the results of the phase-field modeling are still in disagreement with the experimental results in the region of small undercoolings, and the maximum disagreement is observed at the undercooling around $\Delta T \approx 120$ K;

(*ii*) the quantity of impurities on the level of $C_o \approx 0.01$ at.% can strongly influence the growth kinetics in undercooled nickel.

We have used the sharp-interface model of dendrite growth [5, 32] to evaluate the influence of the solute diffusion on growth kinetics and the disagreement between this theoretical prediction and the present experimental data on growth of Nickel dendrites. We have shown, that the solute diffusion effects compensate the disagreement of the theoretical predictions obtained for the thermal convective effects in this region of undercoolings. Using the results of the present phase-field modeling (for evaluation of the effect of convective flow on the dendritic growth) and the sharp-interface model (for evaluation of the solute diffusion effects of

tiny impurities on the dendrite tip velocity), we summarized the contributions from the thermal convection and solute diffusion and then added them to the results of the phase-field model without convection. The final result is shown in Figure 7 in comparison with the present experimental data for free dendrite growth in undercooled nickel melts. Figure 7 shows that we obtain a good agreement with experimental data provided both effects, convection (small and intermediate undercoolings) and solute diffusion (intermediate and large undercoolings) are taken into account. In the region of intermediate undercoolings ≈120-170 K, the summarized effects of convection and solute diffusion completely compensate the disagreement.

Summary

We have presented experimental results of measurements of dendrite growth velocities in undercooled melts of nickel processed containerlessly by electromagnetic levitation chamber. Three different experimental techniques have been applied for these studies to measure the growth dynamics with high reliability at large undercoolings (photo sensors), medium undercooling (capacity proximity sensor) and low undercoolings (high speed CD camera). The sharp interface theory of free dendrite growth developed by Wilfried Kurz et al. has been extended to include effects of fluid flow on mass and heat transport in drops of melts, which are containerlessly processed in alternating electromagnetic fields. The experimental results were analyzed within this model leading to the conclusions that fluid flow in the melt by forced convection due to electromagnetic stirring enhances the growth velocity in the small undercooling range at which the dendrite growth velocity is comparable to the speed of fluid flow. In addition, it is demonstrated that even small amounts of impurities lead to an increase of the growth velocity in the range of small undercoolings at which the growth is then controlled by diffusion of the impurities. The solute effect, however, shows a different temperature characteristics than the transport effect by fluid flow, which makes it possible to discriminate between both these effects by investigating the growth velocities as a function of undercooling.

Acknowledgements

The authors thank Professor Wilfried Kurz for many stimulating discussions, which were helpful and enjoyable during the entire time of collaboration. We also appreciate excellent cooperation with Dr. Matthias Kolbe and fruitful discussions with Professor Alain Karma. Financial support by Deutsche Forschungsgemeinschaft within the priority program SPP1120 “Phase transformations in melts”, contract no HE1601/13, is gratefully acknowledged.

References

[1] W. Kurz and D.J. Fisher, *Fundamentals of Solidification*, 3rd ed. (Trans Tech Publications, Aedermannsdorf, 1992).
[2] J.S. Langer and H. Müller-Krumbhaar, Acta metall**. 26** (1978) 1681.
[3] J. Lipton, W. Kurz, and R. Trivedi, Acta metall. **35** (1987) 957.
[4] M. J. Aziz, J. Appl. Phys. **53** (1982) 1158.
[5] P.K. Galenko and D.A. Danilov, Phys. Lett. A **235** (1997) 271.
[6] T.J. Piccone, Y. Wu, Y. Shiohara, and M.C. Flemings, in: *Solidification Processing,* eds.: J. Beech and H. Jones (The Institute of Metals, London 1988), p. 268.
[7] E. Schleip, R. Willnecker, D.M. Herlach, and G.P. Görler, *Mat. Sci. Eng.* **98** (1988) 39.
[8] D.M. Herlach, *Annu. Rev. Mater. Sci***. 21** (1991) 23.
[9] K. Eckler, M. Kratz, and I. Egry, *Rev. Sci. Instrum,* **64** (1993) 2639.
[10] O. Funke, P. Gandham, M. Kolbe, P. Galenko, and D.M. Herlach, to be published.
[11] K. Eckler and D. M. Herlach, Mat. Sci. Engg. A **178** (1994) 159.

[12] D.M. Matson, in "*Solidification 1998*", M.G. Chu (ed.), Proceedings of the 1998 TMS annual meeting, February 15-19, San Antonio TX, 1998.
[13] K. Eckler, R.F. Cochrane, D.M. Herlach, B. Feuerbacher and M. Jurisch, Phys. Rev. B, **45** (1992) 5019.
[14] C. B. Arnold, M. J. Aziz, M. Schwarz and D.M. Herlach, Phys. Rev B. **59** (1999) 334.
[15] P. Galenko, P.K., O. Funke, J. Wang, D.M. Herlach, Mater. Sci. Eng. A (2003), *in press*.
[16] M. Ben-Amar, Ph. Bouisou, and P. Pelce, J. Cryst. Growth **92** (1988) 97.
[17] Ph. Bouisou, B. Perrin, and P. Tabeling, Phys. Rev. A **40** (1989) 509.
[18] Ph. Bouisou and P. Pelce, Phys. Rev. A **40** (1989) 6673.
[19] V. Emsellem and P. Tabeling, J. Cryst. Growth **92** (1995) 258.
[20] J.-H. Jeong, N. Goldenfeld, and J.A. Danzig, Phys. Rev. E **64** (2001) 041602.
[21] X. Tong, C. Beckermann, A. Karma, and Q. Li, Phys. Rev. E **63** (2001) 061601.
[22] J. Lipton, M.E. Glicksman, W. Kurz, Mater. Sci. Eng. **65** (1984) 57.
[23] J. Lipton, M.E. Glicksman, W. Kurz, Metal. Trans. A **18** (1987) 341.
[24] E. Brener, Zh. Eksp. Teor. Fiz. **97** (1989) 237.
[25] E. Brener, J. Cryst. Growth **99** (1990) 165.
[26] E. Brener and V.I. Melnikov, Adv. Phys. **40** (1991) 53.
[27] J.J. Hoyt, B. Sadigh, M. Asta, and S.M. Foiles, Acta Mater. **47** (1999) 3181.
[28] J.J. Hoyt, M. Asta, and A. Karma, Phys. Rev. Lett. **86** (2001) 5530.
[29] J. Bragard, A. Karma, Y. H. Lee, and M. Plapp, Interface Science **10** (2002) 121.
[30] S.R. Coriell and D. Turnbull, Acta Metall. **30** (1982) 2135.
[31] J.Q. Broughton, G.H. Gilmer, and K.A. Jackson, Phys. Rev. Lett. **49** (1982) 1496.
[32] P.K. Galenko and D.A. Danilov, J. Cryst. Growth **197** (1999) 992.
[33] G.J. Fix, in: *Free Boundary Problems: Theory and Applications*, Eds. A. Fasano and M. Primicerio (Pitman, Boston, 1983) p. 580.
[34] J.B. Collins and H. Levine, Phys. Rev. B **31** (1985) 6119.
[35] J.S. Langer, in: *Directions in Condensed Matter Physics*, Eds. G. Grinstein and G. Mazenko (World Scientific, Philadelphia, 1986) p. 165.
[36] G. Caginalp, Arch. Ration. Mech. Anal. **92** (1986) 205.
[37] A. Karma and W.-J. Rappel, Phys. Rev. E **53** (1996) R3017.
[38] A. Karma and W.-J. Rappel, Phys. Rev. E **57** (1998) 4323.
[39] C. Beckermann, H.-J. Diepers, I. Steinbach, A. Karma, and X. Tong, J. Comp. Physics **154** (1999) 468.
[40] P.K. Galenko, D.M. Herlach, O. Funke, and G. Phanikumar, *in preparation*.